The Astrophysical Journal, 948:128 (15pp), 2023 May 10 https://doi.org/10.3847/1538-4357/acc024

Nonlinear Damping and Field-aligned Flows of Propagating Shear Alfvén Waves with Braginskii Viscosity

Alexander J. B. Russell
School of Science and Engineering, University of Dundee, Dundee, DD1 4HN, Scotland, UK; a.u.russell@dundee.ac.uk
Received 2023 January 10; revised 2023 February 12; accepted 2023 February 27; published 2023 May 16

Abstract

Braginskii magnetohydrodynamics (MHD) provides a more accurate description of many plasma environments than classical MHD since it actively treats the stress tensor using a closure derived from physical principles. Stress tensor effects nonetheless remain relatively unexplored for solar MHD phenomena, especially in nonlinear regimes. This paper analytically examines nonlinear damping and longitudinal flows of propagating shear Alfvén waves. Most previous studies of MHD waves in Braginskii MHD have considered the strict linear limit of vanishing wave perturbations. We show that those former linear results only apply to Alfvén wave amplitudes in the corona that are so small as to be of little interest, typically a wave energy less than 10^{-11} times the energy of the background magnetic field. For observed wave amplitudes, the Braginskii viscous dissipation of coronal Alfvén waves is nonlinear and a factor around 10^9 stronger than predicted by the linear theory. Furthermore, the dominant damping occurs through the parallel viscosity coefficient η_0, rather than the perpendicular viscosity coefficient η_2 in the linearized solution. This paper develops the nonlinear theory, showing that the wave energy density decays with an envelope $(1 + z/L_d)^{-1}$. The damping length L_d exhibits an optimal damping solution, beyond which greater viscosity leads to lower dissipation as the viscous forces self-organize the longitudinal flow to suppress damping. Although the nonlinear damping greatly exceeds the linear damping, it remains negligible for many coronal applications.

Unified Astronomy Thesaurus concepts: Alfven waves (23); Solar corona (1483); Solar coronal heating (1989); Solar coronal holes (1484); Solar wind (1534); Magnetohydrodynamics (1964); Space plasmas (1544); Plasma astrophysics (1261); Plasma physics (2089)

1. Introduction

Alfvénic waves are a ubiquitous feature of natural plasmas, including the solar corona (De Pontieu et al. 2007; Lin et al. 2007; Okamoto et al. 2007; Tomczyk et al. 2007) and solar wind (Coleman 1967; Belcher & Davis 1971). In solar physics, these waves contain sufficient energy to heat the open corona and accelerate the fast solar wind (McIntosh et al. 2011), and they damp significantly within a solar radius above the surface (Bemporad & Abbo 2012; Hahn et al. 2012; Hahn & Savin 2013; Hahn et al. 2022). How these Alfvénic waves damp in astrophysical and space plasmas is an important question that has remained open for almost a century (see early papers by Alfvén 1947 and Osterbrock 1961; modern reviews by Arregui 2015, De Moortel & Browning 2015, and Van Doorsselaere et al. 2020; and historical perspectives by Russell 2018 and De Moortel et al. 2020).

Most theoretical knowledge about solar Alfvénic waves is based on "classical" magnetohydrodynamics (MHD), a mathematical framework that originated from intuitive coupling of Maxwell's equations and the Euler equations of inviscid hydrodynamics (Hartmann 1937; Alfvén 1942, 1943, 1950; Batchelor 1950) and became widely adopted in large part due to its success providing insight into diverse natural phenomena (see, e.g., Priest 2014). However, classical MHD is one member of a larger family of plasma descriptions, some of which offer a more complete description of the plasma. This paper analytically examines Alfvén wave damping in the more general framework of Braginskii MHD, which, unlike classical MHD, retains the anisotropic viscous stress tensor.

A number of authors, including Section 8 of Braginskii (1965), have previously investigated viscous damping of Alfvén waves in the linear limit of vanishingly small wave amplitude. When priority is given to the smallness of the wave amplitude, the problem becomes framed as a matter of how anisotropic viscosity affects velocities that are perpendicular to the magnetic field (the direction of which is treated as unchanging). With this approximation, damping is determined by the "perpendicular" viscosity coefficient η_2, which is extremely small in the corona. It was thus originally concluded that viscous damping is very weak for coronal Alfvén waves unless they have very short wavelengths. This path of reasoning is shown as the vertical branch in Figure 1.

There is, however, another way to view the problem. Viscous damping of Alfvén waves can alternatively be considered with priority given to the largeness of the parallel viscosity coefficient η_0. Given that $\eta_2/\eta_0 \gtrsim 10^{-11}$ is typical in the corona (Hollweg 1985), even a very small component of $\boldsymbol{v}$ parallel to the total magnetic field $\boldsymbol{B}$ would be expected to produce major departures from linear theory. This path of reasoning is shown as the horizontal branch in Figure 1.

The second viewpoint of the problem takes impetus from the observation that (unless wave amplitudes vanish entirely) Alfvén waves do have a nonzero velocity component parallel to the *total* magnetic field. Two effects contribute to this, which are separated if one expands $\boldsymbol{V} \cdot \boldsymbol{B} = \boldsymbol{V} \cdot (\boldsymbol{b} + \boldsymbol{B}_0)$, where $\boldsymbol{B}_0$ is the equilibrium magnetic field and $\boldsymbol{b}$ is the magnetic perturbation. First, $\boldsymbol{V} \cdot \boldsymbol{b}$ is nonzero for an Alfvén wave, since

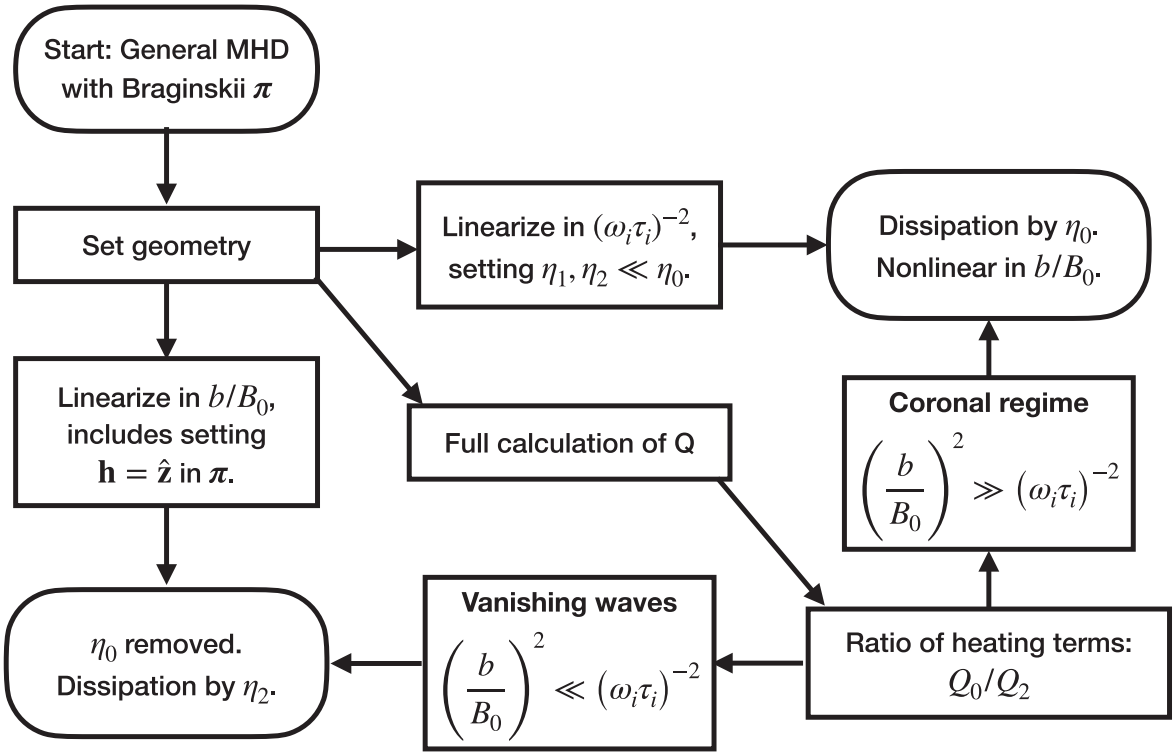

Figure 1. Schematic paths of reasoning. The vertical branch gives priority to the smallness of the wave amplitude and concludes that damping is a linear process governed by the perpendicular viscosity coefficient η_2, e.g., Section 8 of Braginskii (1965). The horizontal branch gives priority to the smallness of η_2/η_0, leading to nonlinear damping via η_0. This paper follows the diagonal branch, which includes deriving the validity condition for the two outcomes. Nonlinear damping via η_0 is appropriate for most coronal applications.

the velocity perturbation perpendicular to $\boldsymbol{B}_0$ is aligned with the magnetic field perturbation $\boldsymbol{b}$. In other words, deflection of the magnetic field from its equilibrium direction implies there is a nonzero velocity component parallel to the *total* magnetic field. Second, in compressible plasma the magnetic pressure of the magnetic field perturbation drives a nonlinear ponderomotive flow parallel to the equilibrium magnetic field (e.g., Hollweg 1971). The ponderomotive flow makes $\boldsymbol{V}\cdot\boldsymbol{B}_0$ nonzero as well. Both of these effects allow for the possibility of nonlinear viscous damping via the large parallel viscosity coefficient η_0.

With the benefit of modern observations (e.g., McIntosh et al. 2011; Morton et al. 2015), it is known that normalized wave amplitudes $b/B_0 \sim V/v_A \sim 0.1$ are typical for the base of an open coronal field region, for example. The "smallness" of the square of this ratio is very modest in comparison to the extreme largeness of η_0/η_2. Thus, it is likely from the outset that viscous damping of Alfvén waves will be a nonlinear process governed by η_0 and the wave amplitude. This paper provides mathematical evidence that this heuristic analysis holds true, along with detailed examination of the consequences.

Various previous studies have explored the effects of Braginskii viscosity on MHD waves since Braginskii (1965). In solar physics, the effect of linearized Braginskii viscosity was revisited from the 1980s to the mid-1990s through the lens of phase mixing and resonant absorption, with the aim of determining how including the viscosity tensor modifies these scale-shortening processes and their heating properties. At the time it was common practice in solar MHD wave theory to work with linearized equations. Thus, due to linearization, Steinolfson et al. (1986), Hollweg (1987), Ruderman (1991), Ofman et al. (1994), and Erdelyi & Goossens (1995) obtained analytical and numerical results that strictly apply to Alfvén waves of vanishing amplitude.

In adjacent fields, the effect of anisotropic viscosity on MHD waves has also been investigated with an eye on MHD turbulence and the solar wind. Of particular note, Montgomery (1992) advocated that Braginskii viscosity is important in hot tenuous plasmas, that in many circumstances it should be treated using parallel ion viscosity, and that plasma motions may self-organize to suppress damping. He further applied these ideas to anisotropy in MHD turbulence, on the basis that a quasi-steady turbulence is composed of the undamped modes. Quantitative elaboration in Montgomery (1992) was based on a linear normal mode analysis, which captures linear damping of magnetoacoustic waves by parallel viscosity, but excludes nonlinear viscous damping of Alfvén waves. The conclusion that a linearized stress tensor damps Alfvén waves only negligibly while damping magnetoacoustic waves significantly was further reinforced by related work by Oughton (1996, 1997).

Similar ideas to ours regarding the importance of nonlinearity were advocated by Nocera et al. (1986), who modeled Alfvén waves subject to the η_0 part of the Braginskii viscous stress tensor, retaining the leading-order nonlinear terms in the wave perturbations. Consistent with the argument above, their calculations found that coronal Alfvén waves damp nonlinearly by parallel viscosity. The current paper complements and extends the previous analysis by Nocera et al. (1986), with the goal of producing a comprehensive understanding of the nonlinear damping and field-aligned flows of propagating shear Alfvén waves with Braginskii viscosity.

A limitation of the mathematical techniques used in this paper is that they exclude certain other nonlinear effects that

may be important in plasmas, such as nonlinear interactions between waves. Numerical investigations will be required in future to verify the analytical theory presented here, compare the relative importance of viscous damping and other nonlinear effects such as parametric decay instability, and consider interactions between nonlinear processes in Braginskii MHD.

This paper is organized as follows. Section 2 provides scientific background on single-fluid Braginskii MHD and its relationship to other single-fluid plasma models. Section 3 quantitatively examines Alfvén wave heating by the full Braginskii viscous stress tensor, demonstrating the importance of nonlinear η_0 terms and compressibility, and obtaining the wave decay properties for the weakly viscous limit using energy principles. In Section 4, we argue that in the highly viscous limit, viscous heating is suppressed by self-organization of the ponderomotive flow, which implies that viscosity strongly alters the field-aligned flow associated with Alfvén waves in this regime. Section 5 further strengthens the analysis, using multiple-scale analysis to obtain the decay properties without restrictions on the Alfvénic Reynolds number, assuming the framework of Braginskii MHD. The paper finishes with a discussion in Section 6 and a summary of the main conclusions in Section 7.

2. Braginskii MHD

Braginskii MHD is an important plasma description that treats anisotropic viscosity and thermal conduction using rigorous closure from physical principles. This section provides a short primer on single-fluid Braginksii MHD, its connection with pressure (or temperature) anisotropy, and its relation to classical MHD and the Chew–Goldberger–Low (CGL) double-adiabatic equations.

As is described in various plasma textbooks, fluid variables can be rigorously and robustly defined as velocity moments of the underlying particle distribution functions. Transport equations for each particle species are then derived by taking moments of the kinetic Boltzmann equation, and combining to obtain the single-fluid equations. Recommended presentations can be found in Schunk & Nagy (2009, their Chapter 7) and the Appendix of Spitzer (1962).

Assuming quasi-neutrality and conservation of mass, momentum, and energy, this process yields the mass continuity equation,

$$\frac{\partial \rho}{\partial t} + \nabla \cdot (\rho \boldsymbol{V}) = 0, \tag{1}$$

the momentum equation,

$$\rho \frac{D\boldsymbol{V}}{Dt} = -\nabla \cdot \boldsymbol{P} + \rho \boldsymbol{G} + \boldsymbol{j} \times \boldsymbol{B}, \tag{2}$$

the energy equation,

$$\frac{D}{Dt}\left(\frac{3}{2}p\right) + \frac{5}{2}p\nabla \cdot \boldsymbol{V} = -\boldsymbol{\pi}\colon \nabla \boldsymbol{V} - \nabla \cdot \boldsymbol{q} + \boldsymbol{j} \cdot (\boldsymbol{E} + \boldsymbol{V} \times \boldsymbol{B}), \tag{3}$$

higher-order transport equations if required, and the generalized Ohm's law.

The pressure tensor $\boldsymbol{P}$ that appears in Equation (2) is the most fundamental representation of the internal forces associated with thermal motions of particles. It is symmetric, so it represents six degrees of freedom. The momentum equation can also be reformulated by introducing the scalar pressure and stress tensor as

$$p = \frac{1}{3}\mathrm{Trace}(\boldsymbol{P}) = \frac{1}{3}P_{\alpha\alpha}, \quad \pi_{\alpha\beta} = P_{\alpha\beta} - p\delta_{\alpha\beta}, \tag{4}$$

where $\delta_{\alpha\beta}$ is the Kronecker delta. So defined, the stress tensor $\boldsymbol{\pi}$ is symmetric and traceless. These definitions give the replacement $-\nabla \cdot \boldsymbol{P} = -\nabla p - \nabla \cdot \boldsymbol{\pi}$.

Deriving transport equations by moment taking meets with a fundamental closure problem: the transport equation for each fluid variable depends on a higher-order variable, producing an infinite regress unless the system can be closed by other considerations. The method of closure is therefore a major distinguishing feature between different fluid models for plasmas. It is also a major source of validity caveats. Various different methods of closure produce governing equations that conserve mass, momentum, and energy, since these properties are already built into Equations (1)–(3). However, the different models discussed below disagree on the internal forces and heating, and can therefore produce different behaviors.

Classical MHD (Hartmann 1937; Alfvén 1942, 1943; Batchelor 1950) corresponds to a closure treatment in which the stress tensor and the heat flow vector are dropped from Equations (2) and (3). Dropping the stress tensor can be justified when particle collisions or other forms of particle scattering such as wave–particle interactions are frequent enough that the pressure tensor remains very close to isotropic. The resulting MHD equations are valid for many situations, for instance modeling static equilibria, or dynamic situations in which the divergence of the stress tensor remains small compared to the Lorentz force. It is nonetheless a truncation since higher-order variables are set to zero rather than approximated. Furthermore, collisionality in environments such as the solar corona is low enough that the stress tensor can become significant for various dynamic phenomena, including MHD waves.

Braginskii MHD uses a less restrictive method of closure. As is detailed by Braginskii (1965), when the collisional mean free path is significantly shorter than the length scales over which fluid quantities vary, the heat flow vector takes the form of an anisotropic thermal conduction and the stress tensor takes the form of an anisotropic viscosity. Closure can therefore be achieved by expressing $\boldsymbol{q}$ and $\boldsymbol{\pi}$ in terms of lower-order fluid variables, which are traditionally derived using methods similar to Chapman & Cowling (1939) or Grad (1949).

The anisotropy inherent in $\boldsymbol{q}$ and $\boldsymbol{\pi}$ can be appreciated heuristically, by considering the helical motion of charged particles in magnetized plasmas. The mean free path parallel to the magnetic field is the same as for unmagnetized plasmas, implying that transport parallel to the magnetic field is the same as for unmagnetized plasmas. Meanwhile, the mean free path perpendicular to the magnetic field is the gyroradius, which is typically much less than the mean free path parallel to the magnetic field, which suppresses perpendicular transport. Hence both thermal conduction and viscous stresses are anisotropic with respect to the magnetic field direction, often extremely so.

The full Braginskii stress tensor, used in Section 3, involves five viscosity coefficients. A useful simplification, used in Section 5, is that for strong magnetizations, $\Omega_i\ \tau_i \gg 1$, the parallel η_0 coefficient greatly exceeds the other viscosity

coefficients. Hence, one can often simplify by neglecting the smaller coefficients (although, as shown in Section 3, it can be necessary to retain other viscosity coefficients if the length scales are highly anisotropic). In this simplification, one has the following covariant expressions for parallel viscosity (Lifshitz & Pitaevskii 1981; Hollweg 1986):

$$\pi_{\alpha\beta} = -3\eta_0\left(h_\alpha h_\beta - \frac{\delta_{\alpha\beta}}{3}\right)\left(h_\mu h_\nu - \frac{\delta_{\mu\nu}}{3}\right)\partial_\mu V_\nu,$$
$$Q_{\rm visc} = 3\eta_0\left(\left(h_\alpha h_\beta - \frac{\delta_{\alpha\beta}}{3}\right)\partial_\alpha V_\beta\right)^2, \quad (5)$$

where $\boldsymbol{h} = \boldsymbol{B}/|\boldsymbol{B}|$ is the unit vector in the direction of the magnetic field. These expressions are different to the isotropic viscosity that appears in the Navier–Stokes equations, owing to the anisotropy introduced by the magnetic field.

Parallel viscosity is closely related to pressure anisotropy. As pointed out by Chew et al. (1956), when $\Omega_i\,\tau_i \gg 1$ the particle Lorentz force makes the pressure tensor gyrotropic, giving it the form

$$P_{\alpha\beta} = p_\perp\,\delta_{\alpha\beta} + (p_{||} - p_\perp)h_\alpha h_\beta. \quad (6)$$

This is a significant simplification, since the six degrees of freedom of a general pressure tensor have been replaced with two variables, $p_{||}$ and $p_\perp$. The definitions in Equations (4) then yield $p = (p_{||} + 2p_\perp)/3$ and

$$\pi_{\alpha\beta} = (p_{||} - p_\perp)\left(h_\alpha h_\beta - \frac{\delta_{\alpha\beta}}{3}\right). \quad (7)$$

Equation (7) shows that pressure anisotropy has an equivalent stress tensor, which is proportional to $p_{||} - p_\perp$. Furthermore, Equations (5) and (7) both have the form $\pi_{\alpha\beta} \sim (h_\alpha h_\beta - \delta_{\alpha\beta}/3)$, so equivalence of the stress tensors reduces to equivalence of the scalar factors in the two equations. An illuminating analysis of the conditions under which they converge has been written by Hollweg (1985, 1986), the most important condition being that collisions (or other processes such as wave–particle interactions) relax the pressure anisotropy driven by velocity gradients to an extent that the pressure is only weakly anisotropic. Classical MHD, for comparison, assumes that pressure anisotropy can be neglected altogether.

For low collisionality, the quasi-static approximation in Braginskii MHD ceases to be valid and strong pressure anisotropy may develop. Under these conditions, separate evolution equations can be derived for $p_{||}$ and $p_\perp$ (Chew et al. 1956; Hollweg 1986). However, the closure problem rears its head again, because those equations depend on the heat flow vector. A simple approach to obtaining a closed system is to ignore the heat flow vector, thus obtaining the CGL double-adiabatic equations (Chew et al. 1956), which are commonly used for collisionless plasma. More sophisticated approaches also exist that solve for the evolution of the pressure anisotropy or the evolution of the stress tensor, retaining the heat flow vector and closing by other means. The works by Balescu (1988), Schunk & Nagy (2009), Zank (2014), and Hunana et al. (2019a, 2019b, 2022) provide further reading on this topic.

In summary, there exists a family of adjacent (sometimes overlapping) single-fluid models for plasmas. The most appropriate choice for a particular problem and/or context depends on the collisionality. When MHD timescales are greater than the ion collision time, Braginskii MHD provides rigorous closure and treats the internal forces and heat flow more accurately than classical MHD.

3. Alfvén Wave Heating by Braginskii Viscosity

3.1. Model

We quantitatively examine the viscous dissipation for an Alfvén wave, which is a transverse wave polarized so that the magnetic perturbation is perpendicular to the equilibrium magnetic field and the wavevector. Setting the equilibrium magnetic field in the z-direction, the magnetic perturbation in the x-direction, and the wavevector in the y–z plane, we consider a total magnetic field of the form

$$\boldsymbol{B} = b(y, z, t)\boldsymbol{e}_x + B_0\boldsymbol{e}_z. \quad (8)$$

This ansatz automatically satisfies $\nabla\cdot\,\boldsymbol{B} = 0$. For the velocity field we assume the form

$$\boldsymbol{V} = V_x(y, z, t)\boldsymbol{e}_x + V_z(y, z, t)\boldsymbol{e}_z. \quad (9)$$

The V_x is the dominant velocity component. In linearized theory it would be the only component of $\boldsymbol{V}$. Additionally, we have explicitly included a higher-order V_z term that represents the nonlinear ponderomotive flow parallel to the equilibrium magnetic field, which is driven by gradients of the magnetic pressure perturbation $b^2/2\mu_0$ associated with a finite-amplitude Alfvén wave (e.g., Hollweg 1971). The V_z term can be dropped when the plasma is incompressible (see Section 3.3). However, it is required for a nonlinear treatment of compressible plasma and affects the wave heating via the parallel viscosity coefficient η_0 (as remarked in Section 1). The expression for V_z in classical MHD is given later in Equation (29).

In a full solution, derivatives of $b^2/2\mu_0$ with respect to y give rise to an additional nonlinear y-component of $\boldsymbol{V}$, which in turn produces a nonlinear y-component of $\boldsymbol{B}$. These terms are not shown explicitly in Equations (8) and (9). Such terms were included by Nocera et al. (1986) and appear not to affect our main conclusions, provided the perpendicular wavelength of the Alfvén wave is sufficiently large.

The viscous force is determined from the viscous stress tensor $\pi_{\alpha\beta}$ by

$$F_{{\rm visc},\alpha} = -\frac{\partial\pi_{\alpha\beta}}{\partial x_\beta}, \quad (10)$$

and the viscous heating rate is determined using

$$Q_{\rm visc} = -\pi_{\alpha\beta}\frac{\partial V_\alpha}{\partial x_\beta}, \quad (11)$$

where $\alpha \in \{x, y, z\}$, $\beta \in \{x, y, z\}$, the x_β are components of the position vector, the V_α are components of $\boldsymbol{V}$, and repeated indices imply summation in the Einstein convention.

A vital point is that the viscous stress tensor depends on the direction of the magnetic field given by the unit vector $\boldsymbol{h} = \boldsymbol{B}/|\boldsymbol{B}|$, which for our Alfvén wave model in Equation (8) has

$$h_x = \frac{b}{\sqrt{B_0^2 + b^2}}, \quad h_y = 0, \quad h_z = \frac{B_0}{\sqrt{B_0^2 + b^2}}, \quad (12)$$

with $h_x^2 + h_z^2 = 1$. Our analysis differs from many past works by considering $h_x \neq 0$ and identifying the dominant heating contribution at the end, as opposed to setting $h_x = 0$ before evaluating the damping effect on Alfvén waves.

Applying formulas from Section 4 of Braginskii (1965; equivalent matrix expressions are given by Hogan 1984), the stress tensor is related to five viscosity coefficients by

$$\pi_{\alpha\beta} = -\sum_{i=0}^{2} \eta_i W_{i\alpha\beta} + \sum_{i=3}^{4} \eta_i W_{i\alpha\beta}. \tag{13}$$

The gyroviscous η_3 and η_4 terms do not contribute to heating, so evaluating the heating rate $Q_{\rm visc}$ requires

$$\begin{aligned} W_{0\alpha\beta} &= \frac{3}{2}\left(h_\alpha h_\beta - \frac{1}{3}\delta_{\alpha\beta}\right)\left(h_\mu h_\nu - \frac{1}{3}\delta_{\mu\nu}\right)W_{\mu\nu}, \\ W_{1\alpha\beta} &= \left(\delta^{\perp}_{\alpha\mu}\delta^{\perp}_{\beta\nu} + \frac{1}{2}\delta^{\perp}_{\alpha\beta}h_\mu h_\nu\right)W_{\mu\nu}, \\ W_{2\alpha\beta} &= (\delta^{\perp}_{\alpha\mu}h_\beta h_\nu + \delta^{\perp}_{\beta\nu}h_\alpha h_\mu)\,W_{\mu\nu}, \end{aligned} \tag{14}$$

where $\delta_{\alpha\beta}$ is the Kronecker delta,

$$\delta^{\perp}_{\alpha\beta} = \delta_{\alpha\beta} - h_\alpha h_\beta, \tag{15}$$

and the rate of strain tensor is

$$W_{\alpha\beta} = \frac{\partial V_\alpha}{\partial x_\beta} + \frac{\partial V_\beta}{\partial x_\alpha} - \frac{2}{3}\delta_{\alpha\beta}\nabla\cdot\boldsymbol{V}. \tag{16}$$

For the shear Alfvén wave geometry described by Equation (9), the $\boldsymbol{W}_i$ tensors become

$$\boldsymbol{W}_0 = \left(h_x h_z \partial_z V_x + \left(\tfrac{2}{3} - h_x^2\right)\partial_z V_z\right)\begin{pmatrix} 3h_x^2 - 1 & 0 & 3h_x h_z \\ 0 & -1 & 0 \\ 3h_x h_z & 0 & 3h_z^2 - 1 \end{pmatrix}, \tag{17}$$

$$\boldsymbol{W}_1 = h_x(h_z\partial_z V_x - h_x\partial_z V_z)\begin{pmatrix} -h_z^2 & 0 & h_x h_z \\ 0 & 1 & 0 \\ h_x h_z & 0 & -h_x^2 \end{pmatrix} + (h_x\partial_y V_x - h_z\partial_y V_z)\begin{pmatrix} 0 & h_z & 0 \\ h_z & 0 & -h_x \\ 0 & -h_x & 0 \end{pmatrix}, \tag{18}$$

$$\boldsymbol{W}_0 = ((1 - 2h_x^2)\partial_z V_x - 2h_x h_z\partial_z V_z)\begin{pmatrix} 2h_x h_z & 0 & 1 - 2h_x^2 \\ 0 & 0 & 0 \\ 1 - 2h_x^2 & 0 & -2h_x h_z \end{pmatrix} + (h_x\partial_y V_x + h_z\partial_y V_z)\begin{pmatrix} 0 & h_x & 0 \\ h_x & 0 & h_z \\ 0 & h_z & 0 \end{pmatrix}, \tag{19}$$

The viscous heating rate with $h_x \neq 0$ retained is thus

$$\begin{aligned} Q_{\rm visc} = {} & \frac{\eta_0}{3}(3h_x h_z\partial_z V_x + (2 - 3h_x^2)\partial_z V_z)^2 \\ & + \eta_1 h_x^2(h_z\partial_z V_x - h_x\partial_z V_z)^2 \\ & + \eta_1(h_z\partial_y V_x - h_x\partial_y V_z)^2 \\ & + \eta_2((1 - 2h_x^2)\partial_z V_x - 2h_x h_z\partial_z V_z)^2 \\ & + \eta_2(h_x\partial_y V_x + h_z\partial_y V_z)^2. \end{aligned} \tag{20}$$

3.2. Two Small Parameters

As anticipated in Section 1 (e.g., Figure 1), two parameters determine the relative importance of individual terms in Equation (20). The first small parameter is $(b/B_0)^2$, the ratio of the wave's magnetic energy density to the energy density of the background magnetic field, which enters through h_x and h_z. In the modern era, extensive observations of coronal MHD waves (Nakariakov & Verwichte 2005; De Moortel & Nakariakov 2012) allow $(b/B_0)^2$ to be quantified with good certainty, directly from resolved wave observations or indirectly from spectral line widths. For example, Morton et al. (2015) studied waves at the base of a coronal open-field region using both approaches and reported a wave speed $v_A = 400\ \mathrm{km\ s^{-1}}$ and wave motions at $v = 35\ \mathrm{km\ s^{-1}}$. Both measurements are consistent with earlier findings for coronal holes and the quiet Sun (e.g., McIntosh et al. 2011). From observations like these, $h_x^2 \sim (b/B_0)^2 \sim (v/v_A)^2 \sim 10^{-2}$.

The second small parameter is $(\Omega_i\tau_i)^{-2}$, which sets the viscosity coefficients η_1 and η_2 relative to η_0. The value of $\Omega_i\tau_i$ can vary significantly in the corona, but if magnetic null points are excluded one obtains values similar to the estimates made by Hollweg (1985), who found 3.4×10^5 for a solar active region and 7.2×10^5 near the base of a coronal hole. We therefore expect $(\Omega_i\tau_i)^{-2} \lesssim 10^{-11}$ under common conditions, and η_1 and η_2 simplify to

$$\eta_2 = \frac{6408}{5125}(\Omega_i\tau_i)^{-2}\eta_0, \quad \eta_1 = \frac{1}{4}\eta_2. \tag{21}$$

The numerical coefficients in Equation (21) are obtained in the limit $(\Omega_i\tau_i)^{-2} \to 0$, e.g., from Equation (73) of Hunana et al. (2022). They are approximate for finite $(\Omega_i\tau_i)^{-2}$ but have a high degree of accuracy because the corrections to the coefficients are of the order of $(\Omega_i\tau_i)^{-2} \lesssim 10^{-11}$. Inspecting Equation (21) and considering $(\Omega_i\tau_i)^{-2} \lesssim 10^{-11}$, the η_2 and η_1 coefficients are both vastly smaller than η_0.

The smallness of $(b/B_0)^2$ and the smallness of $(\Omega_i\tau_i)^{-2}$ compete to make different terms dominate the viscous heating. If one tries to simplify Equation (20) by setting $(b/B_0)^2$ to zero, then $h_x = 0$ and $V_z = 0$ gives $Q_{\rm visc} = \eta_2(\partial_z V_x)^2 + \eta_1(\partial_y V_x)^2$, as obtained by Braginskii (1965). On the other hand, if one tries to simplify by first taking $(\Omega_i\tau_i)^{-2}$ to zero then only η_0 terms remain, suggesting a different conclusion. Thus, the quantitative results recover the two branches shown in Figure 1. To correctly determine the damping under coronal conditions, one must carefully compare terms in the full Equation (20), bearing in mind that there are two small parameters, which we do now (diagonal branch in Figure 1).

3.3. Heating Rate for Incompressible Plasma

The analysis for incompressible plasma is relatively straightforward, which makes it a natural starting point for discussion. The assumption of incompressibility is appropriate for liquid metals or high-beta plasmas, but not, we note, for the corona. The use of coronal wave amplitudes and magnetizations in this section is therefore intended to be instructive only, with the compressible finite-beta treatment that follows later in this paper being required to treat the corona.

In the incompressible case, $\nabla\cdot\boldsymbol{V} = 0$ applied to our Alfvén wave geometry implies $V_z = 0$. Thus, Equation (20) with

$\eta_1 = \frac{1}{4}\eta_2$ simplifies to

$$Q_{\rm visc} = \left\{3\eta_0 h_x^2 h_z^2 + \eta_2\left((1 - 2h_x^2)^2 + \frac{h_x^2 h_z^2}{4}\right)\right\}(\partial_z V_x)^2 + \eta_2\left(\frac{h_z^2}{4} + h_x^2\right)(\partial_y V_x)^2. \quad (22)$$

The terms involving $\partial_z V_x$ set the viscous dissipation due to wavelengths parallel to the equilibrium magnetic field, and we first ask whether dissipation due to parallel wavelengths is dominated by the linear η_2 contribution that has been widely recognized since Braginskii (1965) or the nonlinear η_0 contribution. The ratio of the two terms inside the curly brackets in Equation (22) is

$$3h_x^2\frac{\eta_0}{\eta_2}\left[\frac{1 - h_x^2}{(1 - 2h_x^2)^2 + \frac{1}{4}h_x^2(1 - h_x^2)}\right] \approx 3h_x^2\frac{\eta_0}{\eta_2} \approx 2.4h_x^2(\Omega_i\tau_i)^2, \quad (23)$$

where the first step simplifies using $h_x^2 \ll 1$ (for the observed value of $h_x^2 \approx 10^{-2}$, retaining the terms in the square bracket increases the ratio by 2.8%, so this approximation is both accurate and conservative) and the substitution for η_0/η_2 is by Equation (21). For the coronal wave amplitudes and $\Omega_i\tau_i$ values noted in Section 3.2, this ratio exceeds 10^9, with the nonlinear damping via η_0 dominating the heating rate by that factor. In other words, the viscous dissipation of Alfvén waves via derivatives aligned with the equilibrium magnetic field is a factor 10^9 stronger than predicted by linear theory.

We now evaluate the role of derivatives perpendicular to the equilibrium magnetic field by comparing the nonlinear η_0 term in Equation (22) to the term involving $\partial_y V_x$. The ratio of these heating-rate terms is

$$12h_x^2\frac{\eta_0}{\eta_2}\left(\frac{\lambda_\perp}{\lambda_{||}}\right)^2\left[\frac{1 - h_x^2}{1 + 3h_x^2}\right] \approx 12h_x^2\frac{\eta_0}{\eta_2}\left(\frac{\lambda_\perp}{\lambda_{||}}\right)^2 \approx 9.6h_x^2(\Omega_i\tau_i)^2\left(\frac{\lambda_\perp}{\lambda_{||}}\right)^2, \quad (24)$$

where $\lambda_\perp$ and $\lambda_{||}$ are the wavelengths perpendicular and parallel to the equilibrium magnetic field (for the observed value of $h_x^2 \approx 10^{-2}$, the approximation of the terms in h_x^2 is accurate to 3.9%). For the coronal parameters noted above, if $\lambda_\perp \approx \lambda_{||}$ then the nonlinear η_0 term again dominates by a factor that exceeds 10^9. For smaller transverse wavelengths, the nonlinear η_0 term dominates whenever $\lambda_\perp \gtrsim 10^{-5}\ \lambda_{||}$. If one considers a wave speed of 400 km s^{-1} and a frequency of 3 mHz, consistent with the observations by Morton et al. (2015), the condition that the nonlinear η_0 term dominates becomes $\lambda_\perp \gtrsim 800$ m. Given that the Coronal Multi-Channel Polarimeter (CoMP) instrument has imaged Alfvénic waves using 3 Mm pixels, this condition appears to be met by a very large margin, making the nonlinear η_0 dissipation dominant over the η_2 linear dissipation.

The purpose of deriving Equation (22) and the ratios on the left-hand sides of Equation (23) and (24) such that they include all appearances of h_x and h_z is so that they can be evaluated exactly for a given value of h_x. This makes it explicit that our conclusions are insensitive to the precise value of h_x, requiring only that the value of h_x is broadly consistent with coronal observations. While that approach is most comprehensive, the same conclusions can also be reached by separately simplifying each term in Equation (22) using $h_x^2 \ll 1$ and $h_z^2 = 1 - h_x^2 \approx 1$ to obtain the less cumbersome formula

$$Q_{\rm visc} = \{3\eta_0 h_x^2 + \eta_2\}(\partial_z V_x)^2 + \eta_1(\partial_y V_x)^2, \quad (25)$$

and comparing terms to reach the same conclusions.

3.4. Compressible Plasma with Large Alfvénic Reynolds Number

Under typical coronal conditions, the thermal pressure is too small to prevent compression of the plasma by nonlinear magnetic pressure forces. Thus, a nonlinear V_z develops that is known as the ponderomotive flow (Hollweg 1971). This flow component affects the viscous heating rate via the parallel viscosity coefficient η_0; hence, compressible theory is required for nonlinear viscous damping of Alfvén waves in plasma.

We define the Alfvénic Reynolds number as

$$\mathrm{Re} = \frac{\rho v_A}{k_{||}\eta_0}. \quad (26)$$

This dimensionless parameter differs from the traditional Reynolds number since it refers to the Alfvén speed $v_A = B/\sqrt{\mu_0\rho}$ instead of a typical fluid velocity. This distinction mirrors that between the Lundquist number and magnetic Reynolds number in resistive MHD. Justification for defining Re according to Equation (26) will be found in the detailed mathematical solutions in Section 5, in which it is found to be a natural parameter of the system (see also Nocera et al. 1986).

In this section, the ponderomotive V_z will be related to V_x using expansions in the amplitude of the primary wave fields. Several assumptions are used to accomplish this. First, we make use of the result that a traveling wave solution propagating in the positive z-direction has

$$\frac{\partial}{\partial t} \equiv -v_A\frac{\partial}{\partial z}, \quad (27)$$

where v_A is the wave speed. For simplicity, it is assumed that derivatives of background quantities are sufficiently weak to play a higher-order role in the dynamics. We also simplify here by replacing a full treatment of the thermal conduction with two thermodynamic cases: adiabatic and isothermal. Finally, it is assumed that the Re is large enough that viscous forces can be neglected at leading order when evaluating V_z, which makes it possible to obtain an algebraic relationship between V_z and b^2. This assumption will be removed for Section 5, in which the effect of viscous forces on V_x and V_z is included.

The x-components of the momentum and induction equations are unaffected by the ponderomotive flow at leading order in the wave amplitude. From them one recovers the Walén relation for propagating Alfvén waves, $b/B_0 = -V_x/v_A$.

At leading order, the z-component of the momentum equation is

$$\rho_0 \frac{\partial V_z}{\partial t} + \frac{\partial}{\partial z}\left(\delta p + \frac{b^2}{2\mu_0}\right) = 0, \tag{28}$$

where the viscous force has been neglected since we currently consider the limit of large Re. Using Equation (27) and integrating yields an algebraic relationship between V_z, δp, and b^2. In an adiabatic treatment, the energy equation yields $\delta p = \gamma p_0 \, V_z/v_A$, hence we obtain

$$\frac{V_z}{v_A} = \frac{1}{2(1-\beta)}\left(\frac{b}{B_0}\right)^2, \tag{29}$$

where

$$\beta = \left(\frac{c_s}{v_A}\right)^2 = \frac{\gamma}{2}\left(\frac{p}{B_0^2/2\mu_0}\right). \tag{30}$$

In an isothermal treatment, the ideal gas law $p = \rho RT$ yields $\delta p/p_0 = \delta\rho/\rho_0 = V_z/v_A$. This does not change the form of Equation (29); instead, the isothermal case is recovered simply by setting $\gamma = 1$ in the definition of β.

Defining β as the square of the ratio of the sound speed ($c_s = \sqrt{\gamma p_0/\rho_0}$) to the Alfvén speed differs slightly from the convention of defining β as the ratio of thermal pressure to magnetic pressure, due to the factor $\gamma/2$, which is $5/6$ for an adiabatic monoatomic gas and $1/2$ for an isothermal model. Defining β as the speed ratio squared leads to cleaner mathematics for many MHD wave problems, including this one, and it has therefore become established practice in MHD wave theory.

The $\beta = 1$ singularity in Equation (29) arises because $c_s = v_A$ implies resonance between the Alfvén wave and an acoustic wave, which resonantly transfers energy between the waves. In this specific case, Equation (27) does not apply because it does not account for evolution due to resonance. Similarly, Equation (28) assumes that $V_z \ll v_A$ to simplify the convective derivative, and the solution in Equation (29) does not satisfy this condition in the immediate vicinity of $\beta = 1$. The $\beta = 1$ resonance and the singularity in Equation (29) are not of concern for most coronal applications, which typically have $\beta < 0.2$, but there are special cases in which it is of interest, such as waves propagating toward coronal magnetic nulls or across the $\beta = 1$ layer in the lower solar atmosphere. Russell et al. (2016) have previously applied such nonlinear resonant coupling to the problem of sunquake generation by magnetic field changes during solar flares.

Differentiating Equation (29) and employing the relation $b/B_0 = -V_x/v_A$ yields

$$\partial_\alpha V_z = -\frac{1}{(1-\beta)}\frac{h_x}{h_z}\partial_\alpha V_x, \tag{31}$$

which can be used to eliminate V_z from Equation (20). To leading order in h_x^2 in each viscosity coefficient, we find

$$Q_{\rm visc} = \{C\eta_0 h_x^2 + \eta_2\}(\partial_z V_x)^2 + \eta_1(\partial_y V_x)^2, \tag{32}$$

where

$$C = \frac{1}{3}\left(\frac{1-3\beta}{1-\beta}\right)^2. \tag{33}$$

Some special cases are noteworthy. The incompressible results of Section 3.3 are recovered for $\beta \to \infty$, which gives $V_z \to 0$ and $C \to 3$. Similarly, the cold-plasma solution is recovered by setting $\beta = 0$, which gives $V_z = (b/B_0)^2/2$ and $C = 1/3$.

The nonlinear heating rate for cold plasma ($\beta = 0$) is a factor 9 smaller than for incompressible plasma ($\beta \to \infty$), which demonstrates the importance of compressibility for this problem. Furthermore, $C(\beta)$ is monotonically decreasing between $\beta = 0$ and $\beta = 1/3$. Since $0 < \beta < 1/3$ for most coronal applications, the dissipation rate due to nonlinear Braginskii viscosity in these environments is reduced compared to the cold-plasma solution. For example, given $\beta = 0.1$, the heating rate is approximately 60% of the value for cold plasma. It is therefore evident that compressibility and finite-beta effects must be treated when assessing viscous dissipation of Alfvén waves.

Another important feature is that C has a zero for $\beta = 1/3$. This is one circumstance in which

$$\frac{V_z}{v_A} = \frac{3}{4}\left(\frac{V_x}{v_A}\right)^2 = \frac{3}{4}\left(\frac{b}{B_0}\right)^2, \tag{34}$$

which causes cancellation within the η_0 contribution to $Q_{\rm visc}$. That a particular organization of V_z/v_A can suppress nonlinear viscous dissipation is an important novel finding that Section 4 explores further in the context of low Re.

The final feature of C is the singularity at $\beta = 1$. As noted earlier in this section, $c_s = v_A$ implies that the Alfvén wave is in resonance with a sound wave, which transfers energy between the Alfvén wave and the sound wave. Caution is needed around the resonance, since resonant energy transfer cannot be described using Equation (27), which was used to derive Equation (33).

Evaluation of the ratios of heating terms from Equation (32) proceeds as for the comparison in Section 3.3, but with η_0 multiplied by $C/3$. The top-level conclusions remain intact: heating by the Braginskii viscous stress tensor is dominated by an η_0 term that is nonlinear in the wave amplitude, and for coronal values heating due to the nonlinear η_0 term is many orders of magnitude larger than the heating due to the linear η_1 and η_2 terms.

3.5. What Wave Amplitude Is Linear?

An important implication of the preceding analysis is that nonlinear effects become significant for anisotropic viscosity at far lower wave amplitudes than they do for other terms in the MHD equations. Linearizing the Braginskii viscous stress tensor with respect to the wave amplitude is only appropriate when $h_x^2 \sim (b/B_0)^2 \ll (\Omega_i\tau_i)^{-2}$, which in the corona corresponds to a requirement that the wave energy density is less than 10^{-11} times the energy density of the background magnetic field, far too small to be relevant to coronal energetics. Waves that have small enough amplitudes to be governed by linear viscous damping theory would be unobservable and have no effect on the coronal energy balance. Thus, for coronal Alfvén waves, viscosity must be treated nonlinearly in the wave amplitude, as well as anisotropically

due to the magnetic field. Interestingly, this linearization condition is far more stringent than the linearization condition for other terms in the MHD equations, whereby h_x^2 is normally compared to unity. The extreme difference in these linearization conditions is due to the large η_0/η_2 ratio produced by the strong magnetization.

3.6. Damping Scales for Large Alfvénic Reynolds Number (Energy Derivation)

It is of major interest to know the time and length scales over which waves damp. This section provides a relatively simple derivation of the decay scales for nonlinear viscous damping of propagating shear Alfvén waves for large Re, using energy principles.

Dropping the η_1 and η_2 terms from Equation (32), the heating rate due to the η_0 parallel viscosity coefficient for large Re is

$$Q_{\rm visc} = \frac{\eta_0}{3}\left(\frac{1-3\beta}{1-\beta}\right)^2\left(\frac{b}{B_0}\right)^2(\partial_z V_x)^2. \tag{35}$$

A wave energy decay time can be defined according to $\tau_d = \langle E_w\rangle/\langle Q_{\rm visc}\rangle$, where $\langle . \rangle$ denotes the time average over a wave period, and E_w is the wave energy density. The corresponding decay length is $L_d = v_A\tau_d$.

For forward-propagating Alfvén waves, $E_w \approx \rho_0 V_x^2$ and $V_x = a\cos(\phi)$, where $\phi = k_{||}(z - v_A t)$. Hence,

$$E_w = \rho_0 a^2\frac{(1+\cos(2\phi))}{2}. \tag{36}$$

Similarly, using Equation (35) with $(b/B_0)^2 \approx (V_x/V_A)^2$,

$$Q_{\rm visc} = \frac{\eta_0 k_{||}^2}{3v_A^2}\left(\frac{1-3\beta}{1-\beta}\right)^2 a^4\frac{(1-\cos(4\phi))}{8}, \tag{37}$$

which give the fast time averages:

$$\langle E_w\rangle = \frac{\rho_0 a^2}{2}, \tag{38}$$

$$\langle Q\rangle = \frac{\eta_0 k_{||}^2 a^4}{24 v_A^2}\left(\frac{1-3\beta}{1-\beta}\right)^2. \tag{39}$$

The wave energy decay scales are therefore

$$\tau_d = \frac{12\rho_0}{\eta_0 k_{||}^2 (a/v_A)^2}\left(\frac{1-\beta}{1-3\beta}\right)^2, \tag{40}$$

$$L_d = \frac{12\rho_0 v_A}{\eta_0 k_{||}^2 (a/v_A)^2}\left(\frac{1-\beta}{1-3\beta}\right)^2. \tag{41}$$

Equations (40) and (41) show that waves with larger $k_{||}$ (equivalently, higher frequencies) are damped on shorter scales. We also remark that since L_d depends on the amplitude of V_x (the constant a), the decay envelope is nonexponential. The damping properties are elaborated on more fully in Section 5, in which the assumption of large Re is removed and the functional form of the wave envelope is determined.

4. Self-organized Viscous Flow

In the limit Re→0, the viscous force in the z-component of the momentum equation risks becoming extremely large, unless the flow self-organizes to prevent this. Correspondingly, in the limit Re→0, strong dissipation will prevent waves from propagating, unless V_z is determined by viscosity. One can therefore expect self-organization of the flow pattern for Alfvén waves in highly viscous plasma (small values of Re), which is a concept previously advanced by Montgomery (1992).

To investigate quantitatively, we analyze the highly magnetized regime $\Omega_i\tau_i \gg 1$, simplifying the stress tensor and heating rate by retaining only the η_0 parallel viscosity coefficient. Inspecting Equation (5), the components of $\pi_{\alpha\beta}$ are proportional to $(h_\mu h_\nu - \delta_{\mu\nu}/3)\partial_\mu V_\nu$, and $Q_{\rm visc}$ is proportional to the square of this expression. Applying the shear Alfvén wave geometry of Equations (8) and (9) and simplifying by $h_x^2 \ll 1$,

$$\left(h_\mu h_\nu - \frac{\delta_{\mu\nu}}{3}\right)\frac{\partial V_\nu}{\partial x_\mu} \approx h_x\frac{\partial V_x}{\partial z} + \frac{2}{3}\frac{\partial V_z}{\partial z}. \tag{42}$$

Viscous forces and heating can be suppressed, allowing Alfvén wave propagation, if the flow self-organizes to keep this expression close to zero. Using the Walén relation to substitute $h_x \approx b/B_0 \approx -V_x/v_A$ and integrating, we find that for small Re

$$\frac{V_z}{v_A} = \frac{3}{4}\left(\frac{V_x}{v_A}\right)^2 = \frac{3}{4}\left(\frac{b}{B_0}\right)^2. \tag{43}$$

The relation specified by Equation (43) appeared previously in the different context of Section 3.4, where it was seen that viscous dissipation of Alfvén waves in high-Re plasma is suppressed for the special case of $\beta = 1/3$. The flow pattern required to produce cancellation within the η_0 part of $Q_{\rm visc}$ is independent of Re and β, but it occurs for different reasons in the two cases: in Section 3.4 it arose as a special case of ponderomotive flow with finite beta, and when Re is small it occurs because of self-organization through viscous forces.

This novel result demonstrates that the decay scales and other properties derived in Section 3 should not be extrapolated to small Re. Instead, within Braginskii MHD, as Re→0the viscous force organizes the flow such that V_z obeys Equation (43), for which dissipation is suppressed by cancellation within the η_0 part of $Q_{\rm visc}$.

5. Multiple-scale Analysis

Section 3 used methods of analysis based on heating rates and energy principles. Section 5 now takes a complementary approach of solving the full set of governing equations using multiple-scale analysis in order to reinforce the results of Section 3, extend to general Re by including the effect of the viscous force on $\boldsymbol{V}$, and obtain additional results including the functional form of the nonlinear decay.

5.1. Comparison to Nocera et al. (1986)

We preface the multiple-scale analysis part of this paper with some remarks about related calculations by Nocera et al. (1986). Their work and ours both concentrate on parallel viscosity (η_0) as the main source of wave damping, treating this nonlinearly in the wave amplitude (the horizontal branch of Figure 1). Also in common, both treat ponderomotive and finite-beta effects.

The previous work of Nocera et al. (1986) derived a version of the viscous stress tensor that includes the leading-order effect of $h_x \neq 0$ in the η_0 term. Terms in the viscosity tensor were then compared, concluding like our Section 3 (but by different arguments) that the nonlinear η_0 term exceeds contributions from other viscosity coefficients when

$(b/B_0)^2 \gg (\Omega_i \tau_i)^{-2}$ (their Equation (3.13)). The two studies thus agree on the dominance of nonlinear η_0 viscosity.

Nocera et al. (1986) then found a decay length using the following strategy. A self-consistent perturbation ordering was introduced, then the x-components of the momentum and induction equations were combined to obtain a single equation for V_x, which at linear order is a wave equation. Next, all variables apart from V_x were eliminated from the leading-order nonlinear term. Finally, they concluded from a stability analysis that waves with $k_\perp = 0$ are damped nonlinearly, with a decay time that has the same form as our Equation (40) (their Equation (5.7), given in terms of normalized variables).

The detailed derivation that follows in Section 5.2 draws inspiration from the framework developed by Nocera et al. (1986). We have also taken the opportunity to make several changes that we regard as improvements, most importantly as follows:

1. Nocera et al. (1986) assumed that the fast time average of V_z is zero, which necessitated adding a nonzero constant of integration to V_z. By contrast, we will set the constant of integration to zero, which is the only choice for which an Alfvén wave driver switching on at one boundary does not unphysically send an instantaneous signal to infinity. Additional support for our choice comes from simulations of nonlinear longitudinal flows produced by Alfvén waves (e.g., McLaughlin et al. 2011), which are consistent with the constraint used in our work.
2. The stability analysis in Section 5 of Nocera et al. (1986) is replaced with a multiple-scale analysis of the type covered in Chapter 11 of Bender & Orszag (1978).
3. Nocera et al. (1986) made their wave envelope a function of $z + v_A t$. We treat the envelope as time independent and thus explicitly investigate damping of a propagating wave with respect to distance.
4. Our derivation provides the envelope of V_x as well as the decay length.
5. Our solution is valid for general Re, whereas Nocera et al. (1986) solved for the decay scales in the low-viscosity limit of high Re only.

Equally, Nocera et al. (1986) treated cases that we do not, including the possibility of $k_\perp$ large enough for coupling between the Alfvén and fast modes to alter the wave properties (referred to in their paper as the case of phase-mixed waves).

5.2. Detailed Solution

5.2.1. Geometry and Perturbations

We assume the Alfvén wave geometry of Equations (8) and (9), set $\partial/\partial y \equiv 0$ to concentrate on waves without short perpendicular scales, and introduce density and pressure perturbations $\delta\rho$ and δp together with a self-consistent perturbation ordering that has $V_x/v_A \sim b/B_0 \sim \epsilon^{1/2}$ and $V_z/v_A \sim \delta\rho/\rho_0 \sim \delta p/p_0 \sim \epsilon$. The viscosity η_0 and background quantities B_0, ρ_0, and p_0 are treated as locally homogeneous for simplicity.

5.2.2. Nonlinear Wave Equation

Starting from the ideal induction equation,

$$\frac{\partial \boldsymbol{B}}{\partial t} = \nabla \times (\boldsymbol{V} \times \boldsymbol{B}), \tag{44}$$

we have

$$\frac{\partial b}{\partial t} - B_0 \frac{\partial V_x}{\partial z} = -\frac{\partial}{\partial z}(bV_z) \quad \text{(exact)}, \tag{45}$$

where the linear terms have been grouped on the left-hand side and the nonlinear term has been placed separately on the right-hand side.

The momentum equation is

$$\rho\left(\frac{\partial V_\alpha}{\partial t} + (\boldsymbol{V}\cdot\nabla)V_\alpha\right) = -\frac{\partial}{\partial x_\alpha}\left(p + \frac{B^2}{2\mu_0}\right) + \frac{1}{\mu_0}(\boldsymbol{B}\cdot\nabla)B_\alpha - \frac{\partial \pi_{\alpha\beta}}{\partial x_\beta}. \tag{46}$$

When η_0 contributions dominate the viscous force, Equations (13) and (17) give

$$-\pi_{xz} = 3\eta_0 \frac{b}{B_0}\left(\frac{b}{B_0}\frac{\partial V_x}{\partial z} + \frac{2}{3}\frac{\partial V_z}{\partial z}\right) + O(\epsilon^{5/2}) \tag{47}$$

so the x-component of Equation (46) becomes

$$\frac{\partial V_x}{\partial t} - \frac{B_0}{\mu_0\rho_0}\frac{\partial b}{\partial z} = -\frac{\delta\rho}{\rho_0}\frac{\partial V_x}{\partial t} - V_z\frac{\partial V_x}{\partial z} + \frac{3\eta_0}{\rho_0}\frac{\partial}{\partial z}\left(\frac{b}{B_0}\left[\frac{b}{B_0}\frac{\partial V_x}{\partial z} + \frac{2}{3}\frac{\partial V_z}{\partial z}\right]\right) + O(\epsilon^{5/2}), \tag{48}$$

where linear terms and nonlinear terms have again been placed on opposite sides of the equation.

Taking the time derivative of Equation (48), and using Equation (45) to eliminate b from the linear terms,

$$\left(\frac{\partial^2}{\partial t^2} - v_A^2\frac{\partial^2}{\partial z^2}\right)V_x = -v_A^2\frac{\partial^2}{\partial z^2}\left(\frac{b}{B_0}V_z\right) - \frac{\partial}{\partial t}\left(\frac{\delta\rho}{\rho_0}\frac{\partial V_x}{\partial t} + V_z\frac{\partial V_x}{\partial z}\right) + \frac{3\eta_0}{\rho_0}\frac{\partial^2}{\partial t\partial z}\left(\frac{b}{B_0}\left[\frac{b}{B_0}\frac{\partial V_x}{\partial z} + \frac{2}{3}\frac{\partial V_z}{\partial z}\right]\right) + O(\epsilon^{5/2}). \tag{49}$$

Interpreting Equation (49), the linear terms (on the left-hand side) correspond to a wave equation with wave speed v_A. The leading nonlinear terms (those shown explicitly on the right-hand side) include the leading-order effect of the anisotropic viscosity, which enters at the same order as the leading nonlinear terms that appear in perturbative nonlinear theory of ideal Alfvén waves.

Next, we eliminate b and $\delta\rho$ from the $O(\epsilon^{3/2})$ nonlinear terms in Equation (49). Equations (45) and (48) are solved at linear order by the Walén relation:

$$\frac{b}{B_0} = \pm\frac{V_x}{v_A} + O(\epsilon^{3/2}). \tag{50}$$

We choose the negative sign so waves travel in the positive z-direction, giving

$$\frac{b}{B_0} = -\frac{V_x}{v_A} + O(\epsilon^{3/2}). \tag{51}$$

The traveling wave behavior of the linear solution together with assumption that the wave envelope changes over a distance

controlled by the leading-order nonlinear terms in Equation (49) allows replacement:

$$\frac{\partial}{\partial t} = -v_A \frac{\partial}{\partial z} + O(\epsilon). \tag{52}$$

The density perturbation is governed by the mass continuity equation:

$$\frac{\partial \rho}{\partial t} + \nabla \cdot (\rho \boldsymbol{V}) = 0, \tag{53}$$

which gives for our shear Alfvén wave

$$\frac{\partial \delta\rho}{\partial t} = -\rho_0 \frac{\partial V_z}{\partial z} + O(\epsilon^2). \tag{54}$$

Then, using Equation (52) and integrating,

$$\frac{\delta\rho}{\rho_0} = \frac{V_z}{v_A} + O(\epsilon^2). \tag{55}$$

The constant of integration has been set to zero, for reasons discussed in Section 5.1.

Using these results, Equation (49) becomes

$$\left(\frac{\partial^2}{\partial t^2} - v_A^2 \frac{\partial^2}{\partial z^2}\right) V_x = v_A \frac{\partial^2}{\partial z^2}(V_x V_z) + \frac{3\eta_0}{\rho_0} \frac{\partial^2}{\partial t \partial z}\left(\frac{V_x}{v_A}\left[\frac{V_x}{v_A}\frac{\partial V_x}{\partial z} - \frac{2}{3}\frac{\partial V_z}{\partial z}\right]\right) + O(\epsilon^{5/2}). \tag{56}$$

Now that the problem has been reduced to the two variables V_x and V_z, it is convenient to make the ϵ dependence explicit by introducing dimensionless variables v and w, defined by

$$V_x(z, t) = \epsilon^{1/2} v_A v(z, t), \quad V_z(z, t) = \epsilon\, v_A w(z, t). \tag{57}$$

Expressing Equation (56) in the dimensionless variables v and w, and dropping the nonexplicit higher-order terms from the right-hand side, we seek solutions to

$$\left(\frac{\partial^2}{\partial t^2} - v_A^2 \frac{\partial^2}{\partial z^2}\right) v = \epsilon \left(v_A^2 \frac{\partial^2}{\partial z^2}(vw) + \frac{\eta_0}{\rho_0} \frac{\partial^2}{\partial t \partial z}\left(\frac{\partial v^3}{\partial z} - 2v \frac{\partial w}{\partial z}\right)\right). \tag{58}$$

5.2.3. Multiple-scale Analysis

Equation (58) is now solved using multiple-scale analysis (e.g., Bender & Orszag 1978). Applying this technique, one introduces a new variable, $Z = \epsilon\, z$, that defines a long length scale, and the perturbation expansions

$$v(z, t) = v_0(z, Z, t) + \epsilon\, v_1(z, Z, t) + \ldots, \tag{59}$$

$$w(z, t) = w_0(z, Z, t) + \epsilon\, w_1(z, Z, t) + \ldots. \tag{60}$$

Derivatives are treated using the chain rule as though z and Z were independent variables and setting $dZ/dz = \epsilon$. Thus,

$$\frac{\partial v}{\partial z} = \frac{\partial v_0}{\partial z} + \epsilon\left(\frac{\partial v_0}{\partial Z} + \frac{\partial v_1}{\partial z}\right) + O(\epsilon^2), \tag{61}$$

$$\frac{\partial^2 v}{\partial z^2} = \frac{\partial^2 v_0}{\partial z^2} + \epsilon\left(2\frac{\partial^2 v_0}{\partial Z \partial z} + \frac{\partial^2 v_1}{\partial z^2}\right) + O(\epsilon^2), \tag{62}$$

with equivalent expressions for derivatives of w.

Substituting into Equation (58), collecting ϵ^0 terms, and thus solving the homogeneous wave equation

$$\left(\frac{\partial^2}{\partial t^2} - v_A^2 \frac{\partial^2}{\partial z^2}\right) v_0 = 0, \tag{63}$$

obtains d'Alembert's solution:

$$v_0(z, Z, t) = f(z - v_A t, Z) + g(z + v_A t, Z). \tag{64}$$

For forward-propagating waves, the function g is zero.

The corresponding w_0 is obtained by integrating the z-component of the momentum equation, Equation (46), which gives

$$\frac{V_z}{v_A} = \frac{1}{\rho_0 v_A^2}\left(\delta p + \frac{b^2}{2\mu_0} + \pi_{zz}\right) + O(\epsilon^2). \tag{65}$$

From Equations (13) and (17), we have

$$-\pi_{zz} = 2\eta_0\left(\frac{b}{B_0}\frac{\partial V_x}{\partial z} + \frac{2}{3}\frac{\partial V_z}{\partial z}\right) + O(\epsilon^2). \tag{66}$$

A substitution for the pressure perturbation δp is obtained by integrating the energy equation

$$\frac{\partial p}{\partial t} + \boldsymbol{V} \cdot \nabla p + \gamma p \nabla \cdot \boldsymbol{V} = (\gamma - 1) Q_{\rm visc}. \tag{67}$$

The viscous heating, $Q_{\rm visc}$, is of order $O(\epsilon^2)$, so integration gives the adiabatic relation

$$\frac{\delta p}{p_0} = \gamma \frac{V_z}{v_A} + O(\epsilon^2). \tag{68}$$

Alternatively, one can consider isothermal conditions using $\delta p/p_0 = V_z/v_A$ from the ideal gas law, which is recovered from Equation (68) by setting $\gamma = 1$.

Using Equations (66) and (68), and eliminating b terms using Equation (51), Equation (65) can be expressed as

$$\left(1 - \beta + \frac{4}{3}\frac{\eta_0}{\rho_0 v_A}\frac{\partial}{\partial z}\right) w = \left(\frac{1}{2} + \frac{\eta_0}{\rho_0 v_A}\frac{\partial}{\partial z}\right) v^2, \tag{69}$$

where $\beta = (c_s/v_A)^2$ and the dropped terms are $O(\epsilon)$. When v and w are expanded according to Equations (59) and (60), a formulation identical to Equation (69) connects w_0 and v_0.

Inspecting Equation (69), it is evident that obtaining w for a known v in general requires solving a first-order linear partial differential equation. In the limit where the viscous terms can be neglected, the problem simplifies to the algebraic $w = v^2/2(1-\beta)$ relation used in Section 3.4. Similarly, when the viscous terms dominate, one obtains the $w = (3/4)v^2$ relation for viscously self-organized parallel flow discussed in Section 3.4. For the detailed solution in this section, we retain the complete set of forces that determine V_z, solving the full Equation (69).

The solution is facilitated by considering the special case where v_0 oscillates sinusoidally in time. For the rest of this derivation we therefore set

$$v_0 = A(Z)e^{i\phi} + A^*(Z)e^{-i\phi}, \quad \phi = k_{||}(z - v_A t), \tag{70}$$

where $A(Z) \in \mathbb{C}$ and $*$ denotes the complex conjugate. Representing A in polar form,

$$A(Z) = R(Z)e^{i\theta(Z)}, \tag{71}$$

Equation (70) is equivalent to

$$v_0(z, Z, t) = 2R(Z)\cos(k_{||}(z - v_A t) + \theta(Z)). \quad (72)$$

From inspection, $2R$ is the local amplitude and θ is a phase shift. We have found the complex form in Equation (70) more convenient to work with in the following.

We now solve for the corresponding w_0. Noting that

$$v_0^2 = A^2 e^{2i\phi} + 2|A|^2 + A^{*2} e^{-2i\phi}, \quad (73)$$

where $|A|^2 = AA*$, we seek a solution of the form

$$w_0 = De^{2i\phi} + D^* e^{-2i\phi} + \hat{w}_0. \quad (74)$$

Substituting into Equation (69), terms in e^0 give

$$\hat{w}_0 = \frac{|A|^2}{1 - \beta}, \quad (75)$$

while terms in $e^{2i\phi}$ and $e^{-2i\phi}$ independently give

$$D = \alpha A^2, \quad \alpha = \frac{1}{2}\frac{(1 + 4ik_{||}\eta_0/\rho_0 v_A)}{(1 - \beta + (8/3)ik_{||}\eta_0/\rho_0 v_A)}. \quad (76)$$

The solution for w_0 can also be expressed without complex numbers. Making explicit the real and imaginary parts of $\alpha = \alpha_r + i\alpha_i$, we have the real constants

$$\alpha_r = \frac{1}{2}\frac{(1 - \beta + (32/3)(\mathrm{Re})^{-2})}{((1 - \beta)^2 + (64/9)(\mathrm{Re})^{-2})}, \quad (77)$$

$$\alpha_i = \frac{2}{3}\frac{(1 - 3\beta)(\mathrm{Re})^{-1}}{((1 - \beta)^2 + (64/9)(\mathrm{Re})^{-2})}, \quad (78)$$

where $\mathrm{Re} = \rho_0 v_A/k_{||}\eta_0$, consistent with Equation (26). It is then easily shown that

$$\frac{w_0}{2R(Z)^2} = \alpha_r \cos(2(k_{||}(z - v_A t) + \theta(Z))) - \alpha_i \sin(2(k_{||}(z - v_A t) + \theta(Z))) + \frac{1}{2(1 - \beta)}. \quad (79)$$

To deduce $R(Z)$ and $\theta(Z)$, we return to analyzing Equation (58). The ϵ^1 terms in Equation (58) give the inhomogeneous partial differential equation

$$\left(\frac{\partial^2}{\partial t^2} - v_A^2\frac{\partial^2}{\partial z^2}\right)v_1 = 2v_A^2\frac{\partial^2 v_0}{\partial Z \partial z} + v_A^2\frac{\partial^2}{\partial z^2}(v_0 w_0) + \frac{\eta_0}{\rho_0}\frac{\partial^2}{\partial t \partial z}\left(\frac{\partial v_0^3}{\partial z} - 2v_0\frac{\partial w_0}{\partial z}\right). \quad (80)$$

The v_0 and w_0 terms drive v_1, and the solution for v_1 will have a secular contribution (i.e., one or more terms that grow relative to corresponding solutions of the homogeneous equation) if terms on the right-hand side resonate with the solution to the undriven wave equation. In the specific case where v_0 is given by Equation (70), secular terms in the solution for v_1 will restrict the domain for which v_0 is a valid approximation if the right-hand side of Equation (80) contains $e^{i\phi}$or $e^{-i\phi}$ terms. The central idea in multiple-scale analysis is to solve for the $A(Z)$ that makes the resonance disappear, making v_0 a durable approximation for v.

Using Equations (70) and (74)–(76), the $e^{i\phi}$ terms vanish from the right-hand side of Equation (80) if and only if

$$\frac{1}{A}\frac{dA}{dZ} = -\frac{k_{||}|A|^2}{2}\left[i\left(\alpha + \frac{1}{1 - \beta}\right) + \frac{k_{||}\eta_0}{\rho_0 v_A}(3 - 4\alpha)\right]. \quad (81)$$

The same condition also removes the $e^{-i\phi}$ terms.

Changing to polar form, Equation (71) implies

$$\frac{1}{A}\frac{dA}{dZ} = \frac{1}{R}\frac{dR}{dZ} + i\frac{d\theta}{dZ}. \quad (82)$$

Hence, the real and imaginary parts of Equation (81) yield the real ordinary differential equations

$$\frac{dR}{dZ} = -\frac{\kappa_1}{2}R^3, \quad (83)$$

$$\frac{d\theta}{dZ} = \kappa_2 R^2, \quad (84)$$

where

$$\kappa_1 = k_{||}\left(\frac{k_{||}\eta_0}{\rho_0 v_A}(3 - 4\alpha_r) - \alpha_i\right), \quad (85)$$

$$\kappa_2 = -\frac{k_{||}}{2}\left(\alpha_r + \frac{1}{1 - \beta} - \frac{k_{||}\eta_0}{\rho_0 v_A}4\alpha_i\right). \quad (86)$$

Equations (83) and (84) govern the local amplitude and phase drift of the Alfvén wave, respectively (see Equation (72)).

Our main interest is in $R(Z)$, which determines how the waves decay. Equation (83) is a separable first-order differential equation. The solution is

$$R(Z) = \frac{R(0)}{\sqrt{1 + \kappa_1 R(0)^2 Z}}. \quad (87)$$

For $\kappa_1 > 0$ the wave envelope decays nonexponentially, over a damping length that is inversely proportional to the square of the initial wave amplitude. Having obtained $R(Z)$, the solution for $\theta(Z)$ is obtained by directly integrating Equation (84). Using Equation (87),

$$\theta(Z) = \theta(0) + \frac{\kappa_2}{\kappa_1}\ln|1 + \kappa_1 R(0)^2 Z|. \quad (88)$$

5.2.4. Solution in Original Variables

Having ensured corrections to $v \approx v_0$ remain of order $\epsilon \sim (b/B_0)^2 \ll 1$, the multiple-scale analysis is concluded by using v_0 as the approximation for v. Returning to the original variables,

$$V_x(z, t) = \frac{a_0}{\sqrt{1 + z/L_d}}\cos(k_{||}(z - v_A t) + (\kappa_2/\kappa_1)\ln|1 + z/L_d| + \theta_0), \quad (89)$$

where a_0 is the amplitude of $V_x(0, t)$, θ_0 sets the initial phase of the wave (at $z = 0$, $t = 0$), and

$$L_d = \frac{4}{\kappa_1(a_0/v_A)^2} \quad (90)$$

is the decay length. Using Equations (77), (78), and (85),

$$\kappa_1 = \frac{k_{||}}{3\,\mathrm{Re}}\frac{(1-3\beta)^2}{(1-\beta)^2+(64/9)(\mathrm{Re})^{-2}}, \quad (91)$$

where Re is the Alfvénic Reynolds number for the wave, as defined by Equation (26). Thus,

$$L_d = \frac{12\,\mathrm{Re}}{k_{||}(a_0/v_A)^2}\frac{(1-\beta)^2+(64/9)(\mathrm{Re})^{-2}}{(1-3\beta)^2}. \quad (92)$$

If one neglects the Re^{-2} term in Equation (92), then L_d agrees exactly with the formula in Equation (41) that we derived from energy principles. The formula for L_d in Equation (92) is more general since it was derived without direct assumptions about the value of $\mathrm{Re} = k_{||}\eta_0/\rho_0 v_A$, although the multiple-scale analysis requires that the combination of parameters $k_{||}$, a_0^2, and Re are such that waves damp over a significantly longer scale than the wavelength.

5.3. Nonexponential Decay and Interpretation of the Damping Length

As a general principle, the Alfvén wave energy density $E_w = \rho V_x^2$ decays more rapidly than the perturbation V_x due to the quadratic power. For exponential decay this is reflected in a factor 2 difference in the respective e^{-1} decay lengths. For the nonexponential decay produced by nonlinear viscous damping, the situation is handled differently. The same L_d describes V_x and E_w, although they have different functional forms. The velocity amplitude decays as $(1+z/L_d)^{-1/2}$ (see Equation (89)), while the wave energy density decays as $(1+z/L_d)^{-1}$. Therefore, over a distance L_d the velocity amplitude reduces by a factor $\sqrt{2}$ and the energy density halves.

5.4. Inclusion of Thermal Conduction

The multiple-scale analysis can also be modified to include explicit thermal conduction. Since thermal conduction is highly anisotropic, we include the parallel thermal conduction, setting the heat flow vector to

$$\boldsymbol{q} = -\mathcal{K}_{||}(\boldsymbol{h}\cdot\nabla T)\boldsymbol{h}, \quad (93)$$

where $\mathcal{K}_{||}$ is the coefficient of parallel thermal conduction, and the temperature $T = p/\rho\mathcal{R}$, where $\mathcal{R}$ is the gas constant. The energy equation with heat flow is

$$\frac{\partial p}{\partial t} + \boldsymbol{V}\cdot\nabla p + \gamma p\nabla\cdot\boldsymbol{V} = (\gamma-1)(Q_{\mathrm{visc}} - \nabla\cdot\boldsymbol{q}), \quad (94)$$

which replaces Equation (67).

It follows that $\delta p/p_0$ is related to V_z/v_A by the partial differential equation

$$\left(1+\Lambda\frac{\partial}{\partial z}\right)\frac{\delta p}{p_0} = \left(\gamma+\Lambda\frac{\partial}{\partial z}\right)\frac{V_z}{v_A} + O(\epsilon^2), \quad (95)$$

where

$$\Lambda = \frac{(\gamma-1)\mathcal{K}_{||}}{\rho_0\mathcal{R}v_A} \quad (96)$$

is a conductive length scale. In the limit of weak thermal conduction, $\Lambda\to 0$ gives $\delta p/p_0 = \gamma V_z/v_A$, recovering the adiabatic case treated above. Similarly, for strong thermal conduction, $\Lambda\to\infty$ gives $\delta p/p_0 = V_z/v_A$, recovering the isothermal case.

Introducing a dimensionless pressure variable c, defined by $\delta p = \epsilon p_0\, c(z,t)$, expanding $c(z,t) = c_0(z,Z,t) + \epsilon c_1(z,Z,t) + \ldots$ and setting $c_0 = C e^{2i\phi} + C^* e^{2i\phi} + \hat{c}_0$, the terms in e^0 in Equation (95) yield $\hat{c}_0 = \gamma\hat{w}_0$, and the terms in $e^{2i\phi}$ yield $C = \Gamma D$, where

$$\Gamma = \frac{\gamma + 2ik_{||}\Lambda}{1+2ik_{||}\Lambda}. \quad (97)$$

Solving further, an equation $D = \alpha A^2$, analogous to Equation (76), is obtained but with β replaced by the complex-valued $\Gamma p_0/\rho_0 v_A^2$ in the formula for α. Meanwhile, Equations (75) and (81) are unchanged, retaining the real-valued $\beta = \gamma p_0/\rho_0 v_A^2$. The wave amplitude is therefore governed by results identical to Equations (83) and (85), with the aforementioned change in the definition of α.

6. Discussion

6.1. Optimum Damping

Inspecting Equation (92), the formula for $L_d k_{||}$ has a minimum with respect to the Alfvénic Reynolds number at $\mathrm{Re}=8/(3|1-\beta|)$. Thus, shear Alfvén waves with $k_{||} = 3\rho_0 v_A|1-\beta|/3\eta_0$ are damped in the fewest number of wavelengths, which we refer to as optimum damping. The optimally damped waves have

$$\frac{L_d}{\lambda_{||}} = \frac{32}{\pi}\frac{|1-\beta|}{(a_0/v_A)^2(1-3\beta)^2}. \quad (98)$$

When $\beta\ll 1$, the right-hand side of Equation (98) is approximately 10 divided by the square of the normalized wave amplitude. Hence, while nonlinear viscous damping can in principle damp Alfvén waves in a small number of wavelengths, this requires large amplitudes $a/v_A\sim 1$ or $\beta\sim 1$. For more typically encountered amplitudes $a/v_A\sim 10^{-1}$ and low beta, one finds $L_d/\lambda_{||}\gtrsim 1000$, making nonlinear viscous damping negligible for many coronal situations.

6.2. Viscous Self-organization

The suppression of nonlinear viscous damping for small Re (highly viscous plasma) does not mean that viscous effects are unimportant in this regime. On the contrary, nonlinear damping is suppressed for small Re because viscous forces organize the parallel flow associated with the Alfvén wave to approach the relationship $V_z/v_A = (3/4)(V_x/v_A)^2$. This modification of the parallel flow plays a crucial role in avoiding significant nonlinear damping in highly viscous plasma, when modeled using Braginskii MHD.

6.3. Validity Constraints

Throughout this paper, we have assumed that $\beta\neq 1$ to avoid resonant wave coupling. This condition holds throughout most of the corona, so it is appropriate for our primary applications. Additionally, the multiple-scale analysis in Section 5 uses $\epsilon\sim(V_x/v_A)^2\sim(b/B_0)^2$ as a small parameter, one consequence of which is that the nonlinear damping occurs over a distance considerably greater than the parallel wavelength. As noted in Section 3.2, transverse coronal waves are observed in open-field

regions with $\epsilon \sim 10^{-2}$, making weakly nonlinear theory appropriate for such situations. Obtaining nonlinear viscous solutions in the resonant and strongly nonlinear regimes nonetheless remain interesting future challenges for plasma theory.

The applicability of this paper's results to physical problems is also constrained to conditions under which Braginskii MHD can be rigorously applied. As discussed in Section 2, the traditional derivation of Braginskii MHD assumes that the collisional mean free path is less than the macroscopic length scales. Comparing the mean free path parallel to the magnetic field to the parallel wavelength, this condition can be given as $k_{||}\lambda_{mfp} < 1$, where $\lambda_{mfp} = v_{Ti}\tau_i$, $v_{Ti} = \sqrt{k_B T/m_i}$, and τ_i is the ion collision time. Using the formula (Braginskii 1958, 1965; Hollweg 1985)

$$\eta_0 = 0.96 n k_B T \tau_i, \tag{99}$$

and the definition of Re in Equation (26), one can show that

$$k_{||}\lambda_{mfp} < 1 \;\Leftrightarrow\; \beta^{1/2}\,\mathrm{Re} = \frac{\rho c_s}{k_{||}\eta_0} > 1. \tag{100}$$

In other words, Braginskii MHD requires that the Reynolds number based on the sound speed is greater than unity. One should therefore be cautious about applying small Alfvénic Reynolds number results such as viscous self-organization to real low-beta plasmas.

6.4. Formulas for Applications

For applications to real plasmas, the following formulas are convenient. In cases where the parallel viscosity coefficient is determined by Coulomb collisions,

$$\eta_0 = 0.96 n k_B T \tau_i = \frac{22}{\lambda_C} \times 10^{-17} T^{5/2}, \tag{101}$$

where this formula is stated in S.I. units with T in kelvin, and λ_C is the Coulomb logarithm (e.g., Hollweg 1985). The Alfvénic Reynolds number defined in Equation (26) can then be expressed as

$$\mathrm{Re} = 5.8 \times 10^{20} \lambda_C B^2 f^{-1} T^{-5/2}, \tag{102}$$

also in S.I. units, where $f = v_A k_{||}/2\pi$ is the wave frequency. This formula makes explicit the dependences on frequency, magnetic field strength, and temperature. The Alfvénic Reynolds number is smallest when the plasma has high temperature and low magnetic field strength, and for higher-frequency waves. Finally, we express the damping length in Equation (92) as a function of frequency and the mean square velocity $\langle V_x^2 \rangle = a_0^2/2$, which gives

$$L_d = \frac{3}{\pi} \frac{v_A^3 \,\mathrm{Re}}{f \langle V_x^2 \rangle} \frac{(1-\beta)^2 + (64/9)(\mathrm{Re})^{-2}}{(1-3\beta)^2}. \tag{103}$$

6.5. Waves in a Coronal Open-field Region

Outgoing transverse waves in the magnetically open solar corona contain sufficient energy to heat the open corona and accelerate the fast solar wind (McIntosh et al. 2011; Morton et al. 2015), and they are observed to damp significantly within a solar radius above the Sun's surface (Bemporad & Abbo 2012; Hahn et al. 2012; Hahn & Savin 2013; Hahn et al. 2022). Heating at these altitudes is also thought to be important for producing the observed rapid acceleration of the fast solar wind (Habbal et al. 1995; McKenzie et al. 1995). The problem of how the outgoing waves damp has not been conclusively solved, although one leading hypothesis is turbulent cascade driven by interactions with downgoing Alfvén waves (Hollweg 1986; Heyvaerts & Priest 1992; Matthaeus et al. 1999; Cranmer et al. 2007; Verdini et al. 2010; Mikić & Downs et al. 2018) produced either by reflection from density inhomogeneities (van Ballegooijen & Asgari-Targhi 2016; Pascoe et al. 2022) or by parametric decay instability (Galeev & Oraevskii 1963; Derby 1978; Goldstein 1978; Shoda et al. 2019; Hahn et al. 2022).

Here, we demonstrate that Braginskii viscosity does not cause significant damping of Alfvén waves at the altitudes at which the traditional derivation of Braginskii MHD holds. For concreteness, we consider the Sun's northern polar open-field region on 2012 March 27, using observational values reported by Morton et al. (2015). Enhanced wave power was present around $f = 5$ mHz, which suggests Alfvénic waves produced by p-modes (Morton et al. 2019). We will calculate damping lengths for this frequency, noting that Re and L_d depend on f, with $L_d \sim f^{-2}$ in the limit of high Re. Morton et al. (2015) inferred that the Alfvén speed was nearly constant with $v_A = 400\ \mathrm{km\ s^{-1}}$ on their domain of $r = 1.05$ to $1.20\ R_\odot$. For temperature, we set $T = 1.6$ MK, the formation temperature of the Fe XIII 10,747 Å and 10,798 Å lines used by the CoMP instrument, which implies the proton thermal speed $V_{Ti} = \sqrt{k_B T/m_i}$ is $115\ \mathrm{km\ s^{-1}}$. Hence, for an isothermal equation of state $\beta = 0.083$ and $\beta^{1/2} = 0.29$. For the wave velocity amplitude, Morton et al. (2015) recommended that the reported nonthermal line width should be used, which varies with altitude.

Starting with the lowest altitude observed by Morton et al. (2015), $r = 1.05\ R_\odot$, we set $n = 10^{14}\ \mathrm{m^{-3}}$, $B = 2 \times 10^{-4}$ T, and take the rms value of V_x as $35\ \mathrm{km\ s^{-1}}$. We therefore find $\lambda_C = 19$ and $\mathrm{Re} = 28$. Since $\beta^{1/2}\,\mathrm{Re} = 8 > 1$, Braginksii MHD applies and we evaluate $L_d = 4.2 \times 10^8\ \mathrm{km} \equiv 600\ R_\odot$.

At $r = 1.20$, we set $n = 10^{13}\ \mathrm{m^{-3}}$, $B = 6 \times 10^{-5}$ T, and take the rms value of V_x as $50\ \mathrm{km\ s^{-1}}$. The observed parameters therefore give $\lambda_C = 21$ and $\mathrm{Re} = 2.7$. Since $\beta^{1/2}\,\mathrm{Re} = 0.8 \approx 1$, this altitude is close to the maximum at which the assumptions by which Braginskii MHD is traditionally derived remain valid (for this particular open-field region, and assuming Equation (101)). Evaluating the damping length here returns $L_d = 4.2 \times 10^7\ \mathrm{km} \equiv 61\ R_\odot$.

We conclude that Braginskii viscosity does not cause significant wave damping below $r = 1.2\ R_\odot$, which is consistent with observational results that Alfvénic wave amplitudes in coronal holes follow ideal WKB scaling out to around this altitude (Cranmer & van Ballegooijen 2005; Hahn & Savin 2013).

Between the altitudes we have examined, L_d reduces by an order of magnitude. If one were to extrapolate using high Re or incompressible results, it would appear that viscous damping becomes important near the altitudes at which the waves are observed to damp. We are cautious about making such an assertion for two reasons. First, as discussed in Section 6.1, our results show that for $\mathrm{Re} < 8/(3|1-\beta|)$ the damping length in a Braginskii MHD model increases again as the field-aligned flow self-organizes to supress viscous damping. Second, as the plasma becomes increasingly collisionless ($\beta^{1/2}\,\mathrm{Re} < 1$) the traditional derivation of Bragniskii MHD falters.

Intriguingly, it may be significant that the onset of wave damping broadly coincides with the altitude at which Braginskii MHD can no longer be confidently applied if one invokes the η_0 expression for Coulomb collisions given in Equation (101). This correspondence is suggestive that the wave damping observed in coronal holes may involve collisionless and heat flow effects not found in the most common fluid models.

6.6. Future Work

The present types of analyses should be extended in future to other types of propagating transverse MHD waves. The nonlinear longitudinal flow that accompanies propagating torsional Alfvén waves differs from its counterpart for propagating shear Alfvén waves (Vasheghani Farahani et al. 2011) and it will be of interest to investigate how this difference affects the nonlinear viscous damping. It is similarly desirable to determine how nonlinear viscosity affects propagating kink waves (Edwin & Roberts 1983).

For propagating shear Alfvén waves, viscous damping appears most promising near the $c_s = v_A$ singularity, which must be treated using different methods to those used in this paper. The solar wind frequently has $\beta \sim 1$. Furthermore, $\beta = 1$ occurs in the lower solar atmosphere and in the vicinity of coronal null points. Hence, this case is of considerable physical interest. One challenge for application to magnetic nulls is that the magnetic field unit vector $\boldsymbol{h} = \boldsymbol{B}/|\boldsymbol{B}|$ is not defined at the null itself, so one must be careful to evaluate the Braginskii stress tensor using appropriate calculations; for example, see recent discussion by MacTaggart et al. (2017).

A further challenge is to develop a theory of nonlinear viscous damping applicable to strongly nonlinear waves with amplitudes $b \sim B_0$ and greater. The results of the multiple-scale analysis in Section 5 are rigorous only for the weakly nonlinear case, in which $\epsilon \sim (b/B_0)^2$ can be treated as a small parameter and it is assumed that the damping length is significantly longer than the wavelength. Strongly nonlinear Alfvén waves with $b \sim B_0$ are a feature of the solar wind, and while the low collisionality of the solar wind means that Braginskii MHD may not be an appropriate framework for that application, extending the current work to strongly nonlinear waves remains an interesting problem.

There is a diverse collection of MHD wave problems beyond wave damping for which viscous effects are likely to be significant. Prime among these are nonlinear phenomena involving Alfvén waves, for which the nonlinear viscosity tensor enters the equations at the same order as the effect of interest. For example, standing Alfvén waves drive significantly stronger field-aligned flows than occur for propagating waves because standing Alfvén waves create inhomogeneous time-averaged magnetic pressure. There could also be significant value in investigating how viscosity modifies wave interactions, including Alfvén wave collisions and parametric decay instability (Galeev & Oraevskii 1963; Derby 1978; Goldstein 1978), which are central to leading hypotheses of wave heating in the magnetically open solar corona.

Finally, we point to the continuing need for basic plasma physics research to provide increasingly rigorous derivation and validation of the appropriate fluid equations for weakly collisional and collisionless plasma, in the face of the closure problem summarized in Section 2. As discussed in Section 2 and 6.3, Braginskii MHD breaks down at higher altitudes in the corona as the plasma becomes increasingly collisionless (see Equations (100) and (102)). The CGL double-adiabatic equations and other models that evolve the stress tensor may provide a more suitable framework in these conditions. Hunana et al. (2019a, 2019b, 2022) provide recent discussions of such models and their limitations. Alternatively, it may be necessary for the solar waves community to more widely adopt nonfluid plasma models. However, the tractability of kinetic models remains a limiting factor, especially in light of the large separations between kinetic and macroscopic scales that are characteristic of the Sun's corona. Eloquent comments on these matters can be found in Montgomery (1996).

7. Conclusions

This paper has investigated the properties of propagating shear Alfvén waves subject to the nonlinear effects of the Braginskii viscous stress tensor. The main points are as follows:

1. For many plasma environments, including the low-altitude solar corona, Braginskii MHD provides a more accurate description of the plasma than classical MHD does, by rigorously treating the stress tensor and thermal conduction. Stress tensor effects nonetheless remain relatively unexplored for many solar MHD phenomena.
2. The dominant viscous effects for propagating shear Alfvén waves are nonlinear in the wave amplitude and occur through the "parallel" viscosity coefficient, η_0. Theoretical results based on linearizing the stress tensor with respect to the wave amplitude are only valid for amplitudes satisfying $(b/B_0)^2 \ll (\Omega_i \tau_i)^{-2}$. Such waves would be energetically insignificant under normal coronal conditions, hence nonlinear treatment is required.
3. Compressibility and pressure affect the nonlinear field-aligned flow associated with shear Alfvén waves, hence they impact nonlinear wave damping. Both must be included to produce accurate coronal results.
4. Braginskii viscosity damps propagating shear Alfvén waves nonlinearly, such that the primary wave fields b and V_x decay as $(1 + z/L_d)^{-1/2}$, where the decay length

$$L_d = \frac{12\,\mathrm{Re}}{k_{||}(a_0/v_A)^2}\frac{(1-\beta)^2 + (64/9)(\mathrm{Re})^{-2}}{(1-3\beta)^2}.$$

   Here, a_0 is the initial velocity amplitude of the wave, $\beta = (c_s/v_A)^2$, and $\mathrm{Re} = \rho v_A/k_{||}\eta_0$ is the Alfvénic Reynolds number of the wave. The energy density decays as $(1 + z/L_d)^{-1}$.
5. Optimal damping (the minimum normalized damping length $k_{||}L_d$) is obtained when $\mathrm{Re} = 8/(3|1-\beta|)$. For low-beta plasma and $(a_0/v_A) \lesssim 10^{-1}$, one finds $L_d/\lambda_{||} \gtrsim 1000$, indicating that nonlinear viscous damping is negligible for many coronal situations.
6. The asymptotic behavior that $L_d \to \infty$ in the highly viscous regime $\mathrm{Re} \to 0$ is attributed to self-organization of the parallel flow by viscous forces such that $V_z/v_A \approx (3/4)(V_x/v_A)^2$, which suppresses dissipation.
7. The applicability of the Braginskii MHD solutions to real plasmas is constrained by the traditional derivation of Braginskii MHD assuming that $k_{||}\lambda_{mfp} < 1$, which is equivalent to $\beta^{1/2}\,\mathrm{Re} = \rho c_s/k_{||}\eta_0 > 1$. In other words, Braginskii MHD requires that the Reynolds number based on the sound speed is greater than unity. We

therefore recommend that only the damping results for large Alfvénic Reynolds number should be applied to real coronal plasma, using the simplified formula $L_d = 12\,\mathrm{Re}(1-\beta)^2/(k_{||}(a_0/v_A)^2(1–3\beta)^2)$ that has been derived in this paper by two different techniques: energy principles and multiple-scale analysis.

8. Application to transverse waves observed in a polar open-field region concludes that nonlinear Braginskii viscosity does not cause significant damping of the waves at the altitudes at which the assumptions by which Braginskii MHD is traditionally derived remain valid ($r \lesssim 1.2\,R_\odot$ for the considered region and wave properties). Intriguingly, the observed onset of wave damping broadly coincides with the altitude at which Braginskii MHD can no longer be confidently applied if one invokes the η_0 expression for Coulomb collisions given in Equation (101).

This work was prompted by and benefited from conversations with Paola Testa, Bart De Pontieu, Vanessa Polito, Graham Kerr, Mark Cheung, Wei Liu, David Graham, Joel Allred, Mats Carlsson, Iain Hannah, and Fabio Reale during a research visit to LMSAL funded by ESA's support for the IRIS mission (2018 August) and meetings of the International Space Science Institute (Bern) International Team 355 (2018 November). I am grateful to Peter Cargill, Andrew Wright, Bart De Pontieu, and Paola Testa for comments on an early draft (2019 June), and Declan Diver for encouragment to explore connections with pressure anisotropy. I thank the reviewer for considered and constructive suggestions, and several unnamed individuals for comments that also improved the manuscript. The research made use of the NRL Plasma Formulary, NASA's ADS Bibliographic Services, and the British Library On Demand service, with assistance from librarians at the University of Dundee.

ORCID iDs

Alexander J. B. Russell https://orcid.org/0000-0001-5690-2351

References

Alfvén, H. 1942, Natur, 150, 405
Alfvén, H. 1943, ArMAF, 29B, 1
Alfvén, H. 1947, MNRAS, 107, 211
Alfvén, H. 1950, Cosmical electrodynamics (Oxford: Clarendon Press)
Arregui, I. 2015, RSPTA, 373, 20140261
Balescu, R. 1988, Transport processes in plasmas (Amsterdam: North-Holland)
Batchelor, G. K. 1950, RSPSA, 201, 405
Belcher, J. W., & Davis, L. J. 1971, JGR, 76, 3534
Bemporad, A., & Abbo, L. 2012, ApJ, 751, 110
Bender, C. M., & Orszag, S. A. 1978, Advanced Mathematical Methods for Scientists and Engineers (Berlin: Springer)
Braginskii, S. I. 1958, JETP, 6, 358
Braginskii, S. I. 1965, RvPP, 1, 205
Chapman, S., & Cowling, T. G. 1939, The Mathematical Theory of Non-Uniform Gases (Cambridge: Cambridge Univ. Press)
Chew, G. F., Goldberger, M. L., & Low, F. E. 1956, RSPSA, 236, 112
Coleman, P. J. J. 1967, P&SS, 15, 953
Cranmer, S. R., & van Ballegooijen, A. A. 2005, ApJS, 156, 265
Cranmer, S. R., van Ballegooijen, A. A., & Edgar, R. J. 2007, ApJS, 171, 520
De Moortel, I., & Browning, P. 2015, RSPTA, 373, 20140269
De Moortel, I., Falconer, I., & Stack, R. 2020, A&G, 61, 2.34
De Moortel, I., & Nakariakov, V. M. 2012, RSPTA, 370, 3193
De Pontieu, B., McIntosh, S. W., Carlsson, M., et al. 2007, Sci, 318, 1574
Derby, N. F. J. 1978, ApJ, 224, 1013
Edwin, P. M., & Roberts, B. 1983, SoPh, 88, 179
Erdelyi, R., & Goossens, M. 1995, A&A, 294, 575
Galeev, A. A., & Oraevskii, V. N. 1963, SPhD, 7, 988
Goldstein, M. L. 1978, ApJ, 219, 700
Grad, H. 1949, CPAM, 2, 331
Habbal, S. R., Esser, R., Guhathakurta, M., & Fisher, R. R. 1995, GeoRL, 22, 1465
Hahn, M., Fu, X., & Savin, D. W. 2022, ApJ, 933, 52
Hahn, M., Landi, E., & Savin, D. W. 2012, ApJ, 753, 36
Hahn, M., & Savin, D. W. 2013, ApJ, 776, 78
Hartmann, J. 1937, MFMed, 15, 6
Heyvaerts, J., & Priest, E. R. 1992, ApJ, 390, 297
Hogan, J. T. 1984, PhFl, 27, 2308
Hollweg, J. V. 1971, JGR, 76, 5155
Hollweg, J. V. 1985, JGR, 90, 7620
Hollweg, J. V. 1986, JGR, 91, 4111
Hollweg, J. V. 1987, ApJ, 320, 875
Hunana, P., Passot, T., Khomenko, E., et al. 2022, ApJS, 260, 26
Hunana, P., Tenerani, A., Zank, G. P., et al. 2019a, JPlPh, 85, 205850602
Hunana, P., Tenerani, A., Zank, G. P., et al. 2019b, JPlPh, 85, 205850603
Lifshitz, E. M., & Pitaevskii, L. P. 1981, Physical kinetics Vol. 10 (Amsterdam: Butterworth-Heinemann), 245
Lin, Y., Engvold, O., Rouppe van der Voort, L. H. M., & van Noort, M. 2007, SoPh, 246, 65
MacTaggart, D., Vergori, L., & Quinn, J. 2017, JFM, 826, 615
Matthaeus, W. H., Zank, G. P., Oughton, S., Mullan, D. J., & Dmitruk, P. 1999, ApJL, 523, L93
McIntosh, S. W., de Pontieu, B., Carlsson, M., et al. 2011, Natur, 475, 477
McKenzie, J. F., Banaszkiewicz, M., & Axford, W. I. 1995, A&A, 303, L45
McLaughlin, J. A., de Moortel, I., & Hood, A. W. 2011, A&A, 527, A149
Mikić, Z., Downs, C., Linker, J. A., et al. 2018, NatAs, 2, 913
Montgomery, D. 1992, JGR, 97, 4309
Montgomery, D. 1996, JPlPh, 56, 387
Morton, R. J., Tomczyk, S., & Pinto, R. 2015, NatCo, 6, 7813
Morton, R. J., Weberg, M. J., & McLaughlin, J. A. 2019, NatAs, 3, 223
Nakariakov, V. M., & Verwichte, E. 2005, LRSP, 2, 3
Nocera, L., Priest, E. R., & Hollweg, J. V. 1986, GApFD, 35, 111
Ofman, L., Davila, J. M., & Steinolfson, R. S. 1994, ApJ, 421, 360
Okamoto, T. J., Tsuneta, S., Berger, T. E., et al. 2007, Sci, 318, 1577
Osterbrock, D. E. 1961, ApJ, 134, 347
Oughton, S. 1996, JPlPh, 56, 641
Oughton, S. 1997, JPlPh, 58, 571
Pascoe, D. J., De Moortel, I., Pagano, P., & Howson, T. A. 2022, MNRAS, 516, 2181
Priest, E. 2014, Magnetohydrodynamics of the Sun (Cambridge: Cambridge Univ. Press), doi:10.1017/CBO9780511635342
Ruderman, M. S. 1991, SoPh, 131, 11
Russell, A. J. B. 2018, SoPh, 293, 83
Russell, A. J. B., Mooney, M. K., Leake, J. E., & Hudson, H. S. 2016, ApJ, 831, 42
Schunk, R., & Nagy, A. 2009, Ionospheres: Physics, Plasma Physics, and Chemistry (Cambridge: Cambridge Univ. Press)
Shoda, M., Suzuki, T. K., Asgari-Targhi, M., & Yokoyama, T. 2019, ApJL, 880, L2
Spitzer, L. 1962, Physics of Fully Ionized Gases (2nd ed.; New York: Interscience)
Steinolfson, R. S., Priest, E. R., Poedts, S., Nocera, L., & Goossens, M. 1986, ApJ, 304, 526
Tomczyk, S., McIntosh, S. W., Keil, S. L., et al. 2007, Sci, 317, 1192
van Ballegooijen, A. A., & Asgari-Targhi, M. 2016, ApJ, 821, 106
Van Doorsselaere, T., Srivastava, A. K., Antolin, P., et al. 2020, SSRv, 216, 140
Vasheghani Farahani, S., Nakariakov, V. M., van Doorsselaere, T., & Verwichte, E. 2011, A&A, 526, A80
Verdini, A., Velli, M., Matthaeus, W. H., Oughton, S., & Dmitruk, P. 2010, ApJL, 708, L116
Zank, G. P. 2014, Transport Processes in Space Physics and Astrophysics, Vol. 877 (Berlin: Springer)